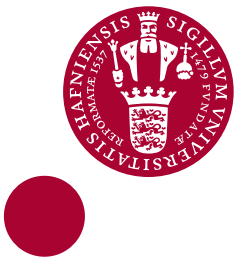

Plasma Proteome Profiling Reveals Dynamics of Inflammatory and Lipid Homeostasis Markers after Roux-En-Y Gastric Bypass Surgery

Wewer Albrechtsen, Nicolai J; Geyer, Philipp E; Doll, Sophia; Treit, Peter V; Bojsen-Møller, Kirstine N; Martinussen, Christoffer; Jørgensen, Nils B; Torekov, Signe S; Meier, Florian; Niu, Lili; Santos, Alberto; Keilhauer, Eva C; Holst, Jens J; Madsbad, Sten; Mann, Matthias

Published in:
Cell Systems

DOI:
10.1016/j.cels.2018.10.012

Publication date:
2018

Document version
Publisher's PDF, also known as Version of record

Article

Cell Systems

Plasma Proteome Profiling Reveals Dynamics of Inflammatory and Lipid Homeostasis Markers after Roux-En-Y Gastric Bypass Surgery

Graphical Abstract

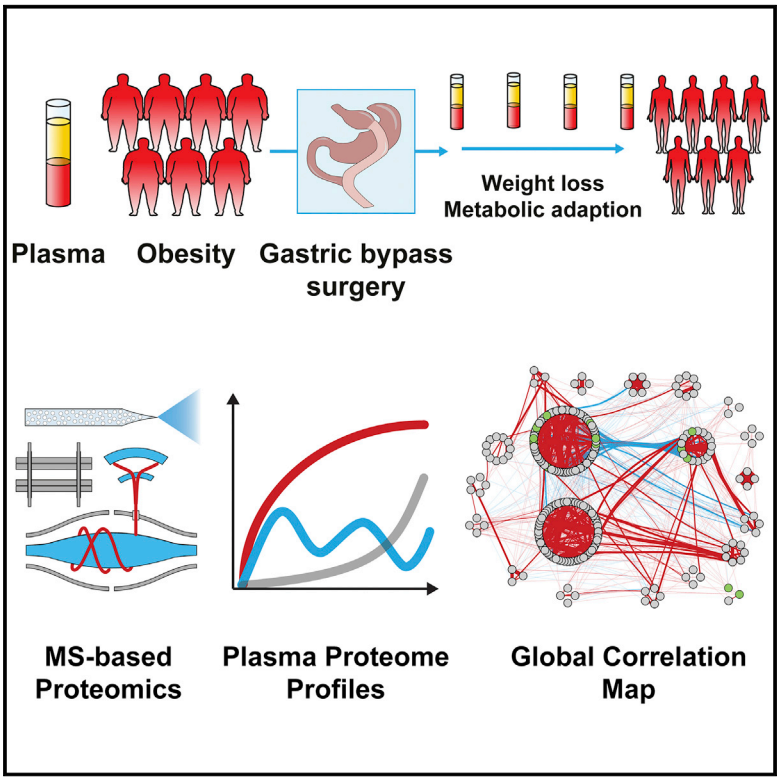

Highlights

- Plasma proteome profiling of independent Roux-en-Y gastric bypass cohorts
- Global correlation maps of the plasma proteome reveal functional networks
- Systemic inflammation and lipid transport are the major remodeled processes
- Gastric bypass has specific and common effects to other weight loss interventions

Authors

Nicolai J. Wewer Albrechtsen, Philipp E. Geyer, Sophia Doll, ..., Jens J. Holst, Sten Madsbad, Matthias Mann

Correspondence

mmann@biochem.mpg.de

In Brief

Bariatric surgery is the most effective intervention in morbidly obese individuals. It is followed by extensive weight loss and improved metabolic health status. We applied plasma proteome profiling, a recently developed mass spectrometric strategy, to quantify the levels of more than 500 circulating proteins in a longitudinal cohort of 47 individuals (total of 1,700 plasma proteins). The resulting global correlation map of the plasma proteome contained about 200,000 relationships and revealed functionally connected protein modules. This determined markers of inflammation, insulin sensitivity, and lipid metabolism.

Wewer Albrechtsen et al., 2018, Cell Systems 7, 601–612
December 26, 2018
https://doi.org/10.1016/j.cels.2018.10.012

CellPress

Cell Systems
Article

Plasma Proteome Profiling Reveals Dynamics of Inflammatory and Lipid Homeostasis Markers after Roux-En-Y Gastric Bypass Surgery

Nicolai J. Wewer Albrechtsen,[1,2,3,4,5,7] Philipp E. Geyer,[1,5,7] Sophia Doll,[1,5] Peter V. Treit,[5] Kirstine N. Bojsen-Møller,[3,6] Christoffer Martinussen,[3,6] Nils B. Jørgensen,[6] Signe S. Torekov,[2,3] Florian Meier,[1,5] Lili Niu,[1] Alberto Santos,[1] Eva C. Keilhauer,[5] Jens J. Holst,[2,3] Sten Madsbad,[3,6] and Matthias Mann[1,5,8,*]

[1]Faculty of Health and Medical Sciences, NNF Center for Protein Research, University of Copenhagen, Copenhagen, Denmark
[2]Department of Biomedical Sciences, Faculty of Health and Medical Sciences, University of Copenhagen, Copenhagen, Denmark
[3]NNF Center for Basic Metabolic Research, Faculty of Health and Medical Sciences, University of Copenhagen, Copenhagen, Denmark
[4]Department of Clinical Biochemistry, Rigshospitalet, University of Copenhagen, Copenhagen, Denmark
[5]Department of Proteomics and Signal Transduction, Max Planck Institute of Biochemistry, Martinsried, Germany
[6]Department of Endocrinology, Hvidovre Hospital, University of Copenhagen, Hvidovre, Denmark
[7]These authors contributed equally
[8]Lead Contact
*Correspondence: mmann@biochem.mpg.de
https://doi.org/10.1016/j.cels.2018.10.012

SUMMARY

Obesity-related diseases affect half of the global population, and bariatric surgery is one of the few interventions with long-lasting weight loss and cardiometabolic effects. Here, we investigated the effect of Roux-en-Y gastric bypass surgery on the plasma proteome, hypothesizing that specific proteins or protein patterns may serve as key mediators and markers of the metabolic response. We performed mass spectrometry (MS)-based proteomics on two longitudinal studies encompassing 47 morbidly obese patients, generating quantitative information on more than 1,700 proteins. A global correlation matrix incorporating about 200,000 relationships revealed functional connections between proteins and assigned them to physiological processes. The main classes of significantly altered proteins were markers of systemic inflammation and those involved in lipid metabolism. Our data highlight robust correlative and anti-correlative behaviors of circulating proteins to each other and to clinical parameters. A group of inflammation-related proteins showed distinct inverse relationships to proteins consistently associated with insulin sensitivity.

INTRODUCTION

Over 600 million people are obese (BMI > 30 kg/m^2) and a further 1.3 billion overweight (W.H.O., 2016). The proportion of the latter subgroup has doubled since 1980, representing an unprecedented number of people predisposed to or already affected by a broad spectrum of co-morbidities (GBD 2015 Obesity Collaborators et al., 2017). These include type 2 diabetes (T2D), cardiovascular disease, endocrine disturbances, neurodegenerative diseases, and several types of cancers.

In response to this global and dramatically increasing burden, the scientific community has devoted substantial efforts to obesity and its clinical consequences, aiming to gain a deeper understanding of the underlying disease mechanisms while developing new treatment possibilities. From a vast array of dietary, behavioral, and pharmacological alternatives, bariatric surgery has emerged as the most effective intervention for treating obesity and T2D. There are different bariatric procedures, with Roux-en-Y gastric bypass (RYGB) among the most established ones, where the creation of a small gastric pouch and bypass of the stomach and upper small intestine, causes accelerated entry of nutrients into the small intestine (Griffen et al., 1977; Mason and Ito, 1967; Mason et al., 1975; Wittgrove et al., 1994). Besides major weight loss (on average 40 kg), the physiological responses to RYGB include broad improvements in cardiovascular status and other measures of metabolic health (Aab et al., 2016; Adams et al., 2017; Cardoso et al., 2017; Madsbad and Holst, 2014; Sjöström et al., 2007). Interestingly, RYGB strongly increases insulin sensitivity for many individuals suffering from T2D. Hepatic insulin sensitivity tends to improve markedly within a week after surgery, even before substantial weight loss, followed by increased sensitivity in peripheral tissues in weeks (Bojsen-Møller et al., 2014). While gastrointestinal peptides, bile acids, and even the microbiome have been implicated in the rapid and drastic physiological changes after RYGB, the molecular mechanisms are poorly understood (Cummings and Rubino, 2018; Miras and le Roux, 2013).

Metabolic processes are regulated by proteins, and the technology of choice to study changes in the proteome in an unbiased manner is mass spectrometry (MS)-based proteomics (Aebersold and Mann, 2016). Proteins circulating in the blood can be both mediators of organ cross talk and markers of whole-body states. However, a system-wide approach has only recently become possible due to technological improvements of the proteomic pipeline (Geyer et al., 2017). We recently

developed "plasma proteome profiling" as a robust and automated platform for the reproducible analysis of hundreds of clinical samples. The quantified proteome included the main functional plasma proteins such as the complement system, apolipoproteins, and other transporters and allowed assessment of sample quality (Geyer et al., 2016a). In a subsequent study, we investigated the longitudinal effects of caloric restriction-induced weight loss on the plasma proteome of 52 individuals over more than a year. Analysis of more than 1,000 individual plasma proteomes revealed that protein levels in general were much more stable within individuals over time than between them. We extracted panels indicative of systemic inflammatory status, allowing stratification of the cohorts. The data also highlighted specific proteins correlated to relevant clinical parameters such as BMI, high-density lipoprotein (HDL), low-density lipoprotein (LDL) and insulin sensitivity (Geyer et al., 2016b).

Here, we wished to gain further insights into the global metabolic changes caused by RYGB surgery as reflected in the plasma proteome. To obtain robust and generalizable results, we selected two studies with similar design to investigate improvements in hepatic insulin sensitivity and beta cell function (Bojsen-Møller et al., 2014; Martinussen et al., 2015). We applied an improved version of our plasma proteome profiling pipeline, which doubled our coverage of the plasma proteome. Furthermore, for a more comprehensive understanding of the dynamics of the plasma proteome, we implemented global correlation maps. These consist of hundreds of thousands of protein-protein connections and protein-clinical parameter associations, highlighting co-regulated proteins and revealing underlying physiological mechanisms.

RESULTS

In-Depth Dataset of the Human Plasma Proteome in RYGB

Study 1 consisted of 20 and study 2 of 27 morbidly obese individuals, with BMI 40 ± 4 kg/m^2 (Bojsen-Møller et al., 2014) and 42 ± 4 kg/m^2 (Martinussen et al., 2015), respectively (Figure 1A). Blood was drawn at four time points, once directly before and three times after surgery (0, 1, 12, and 52 weeks). From 19 individuals, we also obtained blood samples at 2 or 4 years post operation (>104 weeks).

Weight declined steadily in the cohorts, stabilizing at an average loss of 28% of total body mass 1 year after surgery (Figure 1A). Insulin resistance of the liver as estimated by homeostatic model assessment of insulin resistance (HOMA-IR), decreased from 3.3 ± 0.7 to a near normal value of 2.0 ± 0.9 after 12 weeks.

In this study, we further improved the plasma proteome profiling pipeline by first generating deep plasma libraries by consecutive depletions of pooled plasma from the top6 and the top14 highest abundant proteins. Following depletion, we used the recently developed high-pH reversed-phase "spider fractionator" (Kulak et al., 2017) to generate a deep library of 1,928 plasma proteins and 14,588 peptides (excluding contaminants) (Figure 1B). Cohort samples were automatically prepared without any depletion as described previously (Geyer et al., 2016a) (Figure 1C). The second improvement of our workflow was a new acquisition method termed BoxCar, which results in about a 10-fold increase in dynamic range of peptide signals via an equalized filling pattern of the ion trap. This results in substantial coverage of undepleted plasma samples even without fractionation (Meier et al., 2018), which is visually reflected in isotope patterns detected in the *m/z* retention time plane for the full scans (Figure S1).

We generated a large plasma proteome dataset, comprising a total of 175 human plasma proteomes. In triplicate analysis of the samples, an average of 1,025 proteins was identified per study participant, more than twice the number in our previous plasma proteome study (Geyer et al., 2016b) (Figure 1D; Table S1). In total, we quantified 1,700 plasma proteins with at least two peptides in the study samples (Figures 1D and 1E). We also evaluated the cohorts based on our previously defined sets of quality markers. None of the samples suffered from extensive erythrocyte lysis or partial coagulation, but we observed a slight trend toward higher erythrocyte lysis in study 2 (Figure S2).

As this is the largest proteome dataset generated by unbiased MS-based proteomics on non-depleted plasma, we provide the data in an easily accessible and minable format for use by the community (Table S1). Ranking the proteins according to their abundance and annotating them according to their function using the Gene Ontology biological process (GOBP) terms and performing an one-dimensional annotation enrichment analysis resulted in 117 statistically significant terms (Figure 1F). At this depth of coverage, processes connected to lipid transport, coagulation, and inflammation are very well reflected in the higher abundance ranges, whereas intracellular processes — presumably as a result of tissue leakage — are enriched in the low abundance ranges (Table S2).

Plasma Proteome Rearranges after RYGB

Our primary aim was to investigate plasma proteome dynamics after RYGB and to relate these to the pathophysiological changes stemming from the procedure. Over the entire time course, the levels of 114 proteins changed significantly (Table S3). We expected the surgery intervention itself to have a strong effect on the plasma proteome. Indeed, most of the significantly altered proteins — 88 in total — changed 1 week after surgery; 39 proteins after 12 and 52 weeks; and 33 proteins after more than 2 years. The two longitudinal studies differed only minimally in their design, allowing us to initially use study 1 as the "discovery cohort" and study 2 as the "validation cohort" according to the "rectangular strategy" for plasma proteome profiling (Geyer at al., 2017). For the first two time points, where the number of samples was most comparable, 90% of the significantly changed proteins in study 1 were also significant in study 2 (Table S3). Due to the high overlap of proteins regulated in the two independent RYGB studies and the fact that we did not detect any significant differences between them, we henceforth integrated the data from both of them.

To investigate plasma proteome dynamics after RYGB, we calculated the median, *Z*-scored intensities of all significantly altered proteins at each time point. A hierarchical clustering analysis stratified proteins into four main groups based on their response to RYGB (Figures 2A and 2B). Nearly half of these proteins showed a long-term decrease (group 1, 10 proteins; group 2, 40 proteins). The main difference between the two patterns was that group 2 increased at the first post-operative time point before dropping below baseline levels for the entire period of up to 4 years. The 39 proteins in group 3 showed a long-term

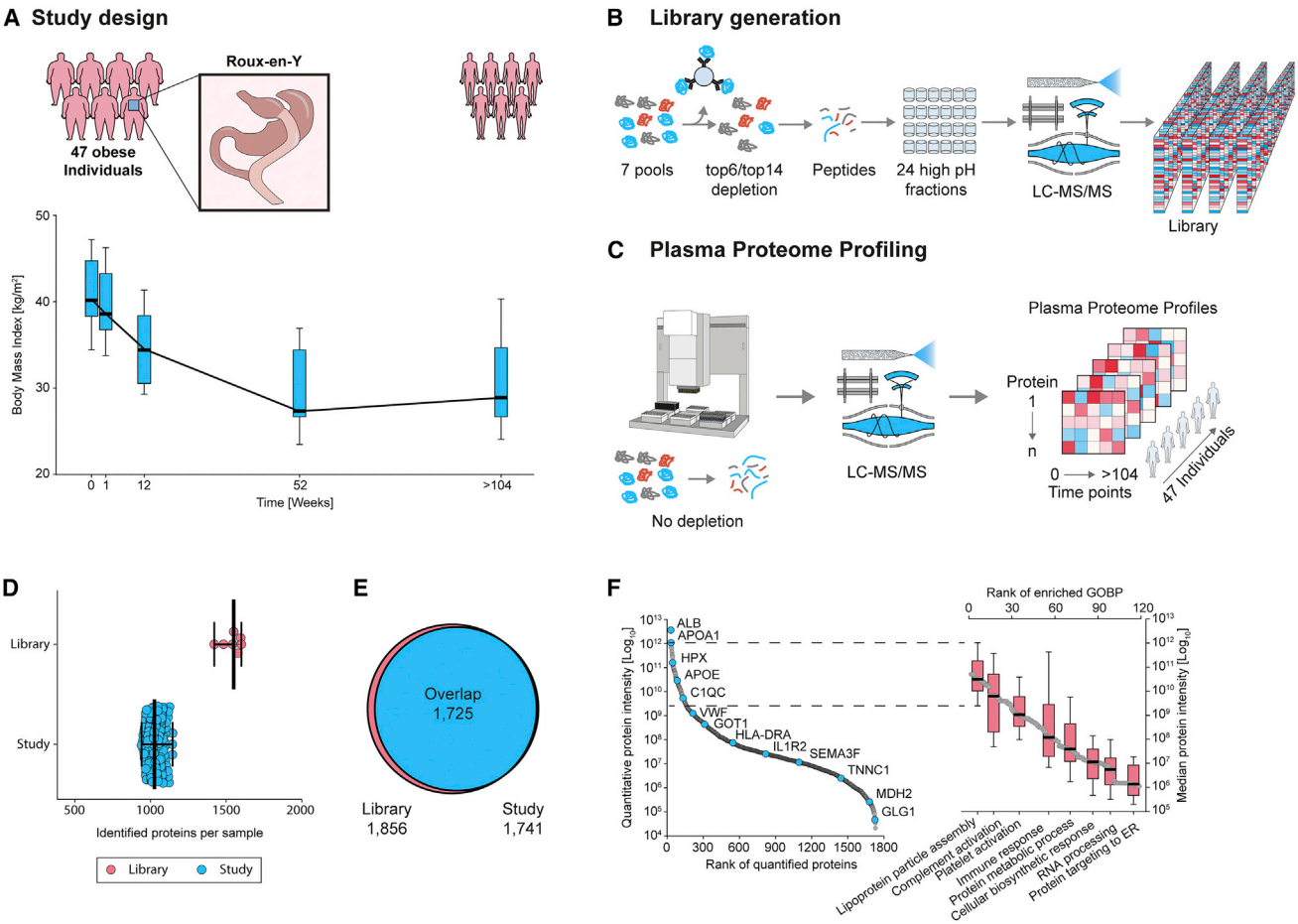

Figure 1. Study Design and Analytical Performance

(A) The two studies involved 47 patients who have undergone Roux-en-Y gastric bypass. The boxplots for the BMI distribution indicate a 10–90 percentile, and the median is highlighted with a black bar.

(B) Highly abundant proteins were only depleted for the library generation in seven pools of plasma. After digestion, peptides were separated at high pH on a reversed phase material into 24 fractions.

(C) Plasma proteome profiling pipeline applied to 175 plasma proteomes in triplicate. Sample preparation took a total of 4 hr, and 45-min gradients were used, resulting in a 3D data matrix of quantified proteins as a function of individuals over time.

(D) Number of identified proteins in each of the seven library pools (red dots) and the 175 plasma samples (blue dots).

(E) Total number of proteins identified in the library and in the study cohort.

(F) Quantitative values of 1,700 plasma proteins ranked according to their abundance. Several proteins are exemplified over the abundance range (blue dots). Functional annotation and 1D enrichment resulted in 117 significantly enriched annotation terms (right graph, gray dots). Eight of these categories are highlighted as boxplots with a 10–90 percentile.

increase, with many of them initially exhibiting a decrease after surgery. This was also the pattern of group 4, although here levels only recovered to baseline. The remaining proteins had a more heterogeneous behavior with increased or decreased levels between the different time points.

We annotated each of the 114 significantly changed proteins with GOBP, molecular function (GOMF), and cellular compartment (GOCC) as well as UniProt-KB keyword terms, to reveal the biological processes that were influenced by RYGB. Fisher's exact test on these keyword annotations yielded 322 connections based on 20 central keywords, drawing a broad picture of biological functions affected by RYGB (STAR Methods; Table S4). These range from inflammation, lipid homeostasis, and protease activity to changes in metal homeostasis.

Next, we performed hierarchical clustering on a Boolean table of the proteins annotated by the 20 keywords, to investigate if proteins belonging to the same cluster also had a functional association (Figure 2C). Terms related to inflammation were most strongly enriched (cluster 2). Manual inspection revealed even more inflammatory proteins, including a frequently clinically used marker of inflammation, C-reactive protein (CRP), the acute phase proteins SAA1, SAA4, and lipopolysaccharide binding protein (LBP), and the complement factors C1S, CFHR3, and CFHR5. The second most keyword-enriched group belonged to the lipid homeostasis system (cluster 3), as expected upon weight loss, and their individual dynamics will be described below.

"Metal binding" was also significantly enriched, but spread over clusters 1, 2, and 3, indicating that RYGB differently

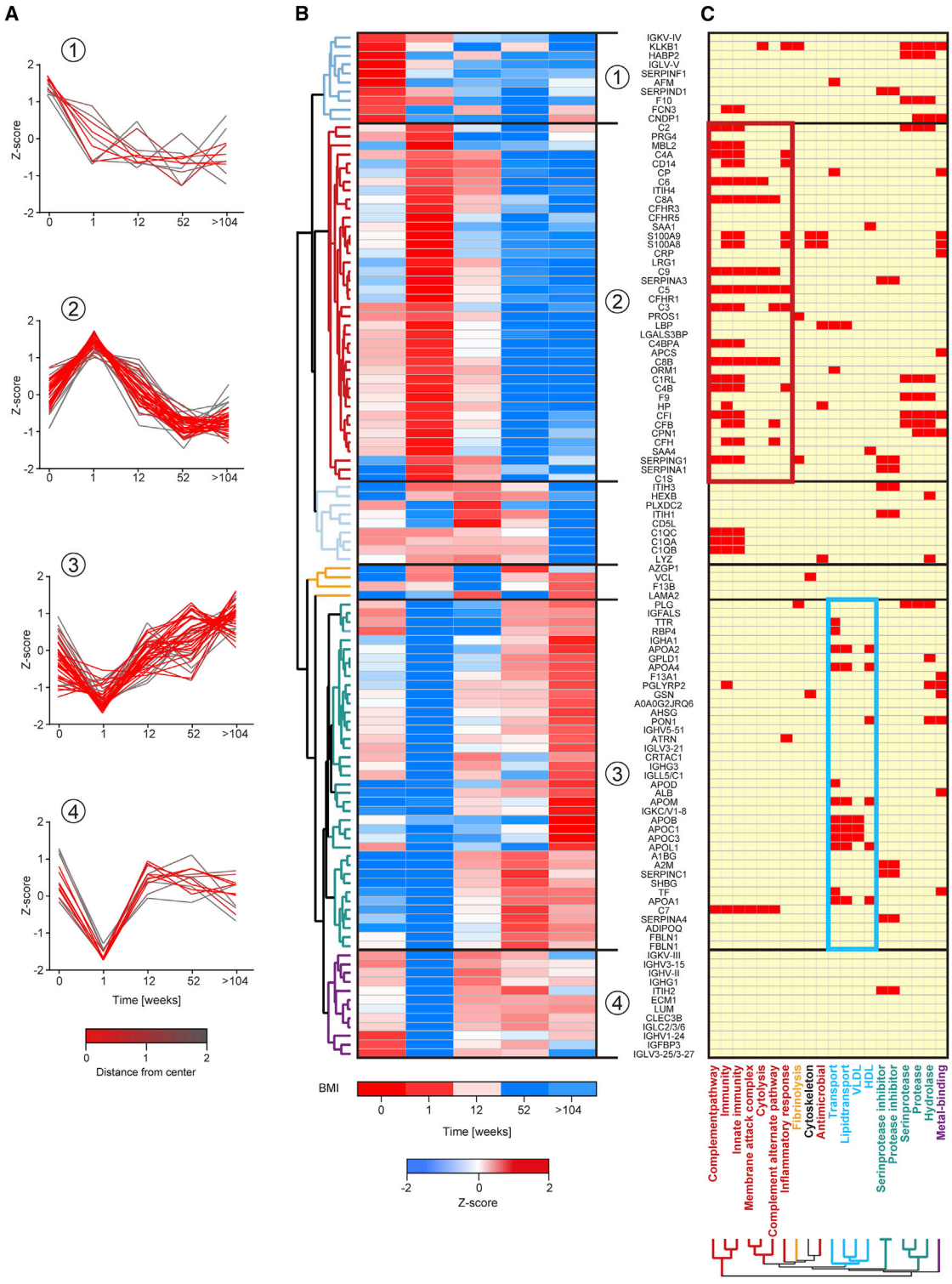

Figure 2. Longitudinal Trajectories and Functional Interpretation of Significantly Influenced Proteins

(A) Proteins clustered into four main groups according to their patterns of adaption after RYGB. *Z*-scores are plotted over five time points.

(B) Hierarchical clustering of the plasma proteins in the four groups.

(C) A Fisher's exact test identified 20 main keywords, which were used in a second hierarchical clustering analysis for functional interpretation of the longitudinal trajectories. The dominant keywords — related to inflammation and the lipid homeostasis system — are highlighted by red and blue rectangles, respectively.

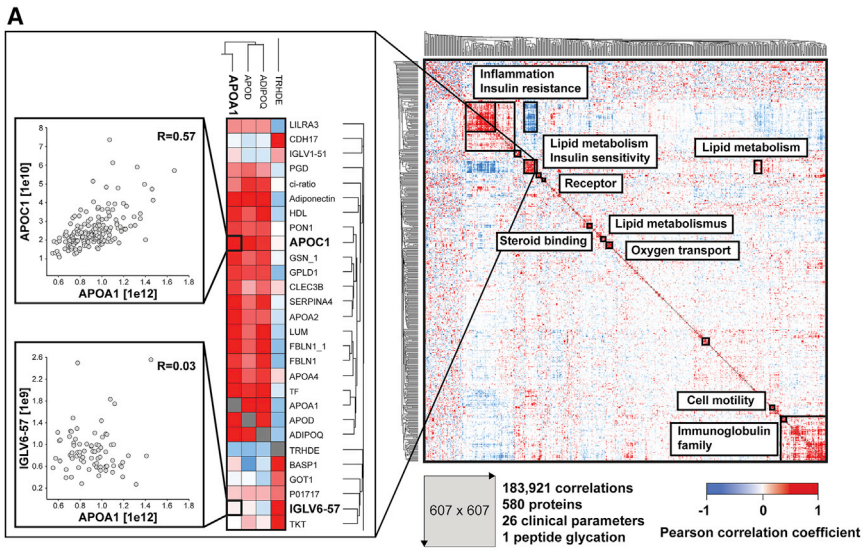

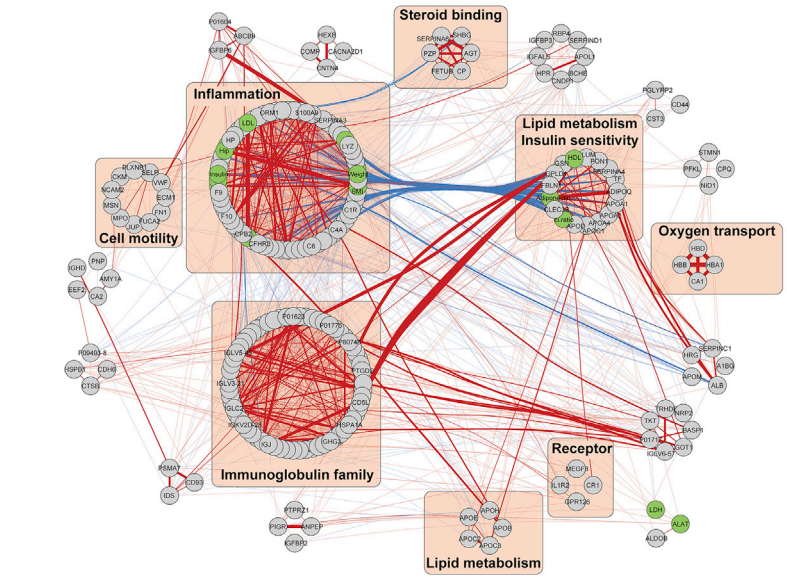

Figure 3. Global Correlation Map of the Plasma Proteome

(A) Pairwise correlation of proteins using their intensity levels over the 175 study samples results in a matrix of correlation coefficients where one protein is compared to all other proteins and clinical parameters. The left panel illustrates the calculation of the Pearson correlation coefficient between two proteins with high and low correlation, respectively. The right-hand panel shows cross-correlations of all quantified proteins and clinical parameters (25% valid values) after subsequent hierarchical clustering, revealing an extensive map of co-regulated items (proteins, clinical parameters, peptide glycation). In the map, items with a strong correlation or anti-correlation to each other cluster together in red or blue areas, respectively. The main clusters are functionally annotated with keywords.

(B) Network analysis of the main clusters in (A) reveals connections within and between them. The thickness of the lines corresponds to the Pearson correlation coefficient (red lines: positive correlations; blue lines: anti-correlations; green cycles: clinical parameters).

affected their functional roles (Table S4). The absorption of iron is compromised after gastric bypass surgery since the antrum, duodenum, and the proximal part of the jejunum, where absorption takes place is separated from the contact with the ingested nutrients and results in anemia, due to malabsorption of micronutrients (Worm et al., 2015). Interestingly, levels of transferrin (TF), the main iron transporter in plasma, increased by 20% (cluster 3), indicating a sensing mechanism for low iron levels. In contrast, ceruloplasmin (CP), which oxidizes Fe2+ to Fe3+ for effective transport by TF, was downregulated and present in cluster 2, which anti-correlates with cluster 3, perhaps because less iron needs to be oxidized.

We traced the significantly regulated proteins connected to protease keyword annotations to members of the complement cascade system and different serine protease inhibitors (SERPINs). SERPINs are a functionally heterogeneous group of proteins, including the inflammation-associated SERPINA1 and SERPINA3 (cluster 2) and also the adipocyte-secreted SERPINF1, whose decrease after operation indicates the loss of body fat (cluster 1).

Encouraged by the fact that plasma proteome profiling revealed specific physiologic changes upon RYGB, we set out to systematically exploit the observed regulation to construct a global network of co-regulated plasma proteins and functional modules.

Global Correlation Maps Reveal Co-regulation of Hundreds of Plasma Proteins

The levels of plasma proteins have traditionally been measured and considered independently; however, proteins often work together as complexes or groups. Treating RYGB as a generic perturbation, we next investigated the co-regulation of the plasma proteome at a systems level to identify protein networks and search for new biomarker candidates. We constructed a global correlation map containing pairwise relationships between all proteins and further included clinical parameters. In our case, there were up to 175 abundance values for each plasma protein (47 individuals; 5 time points). For instance, the Pearson correlation coefficient between the apolipoprotein proteins APOA1 and APOC1 was 0.57 over all data points (Figure 3A).

We considered only the 580 proteins that were quantified in at least 25% of the samples and added 26 clinical parameters. As a third parameter group, we included the levels of glycated peptides, which are related to blood sugar control and can be determined by proteomics as previously described (Keilhauer et al.,

2016). Here, we quantified 203 glycated peptides and combined them into a single ''peptide glycation'' factor (STAR Methods). The protein abundance levels, clinical parameters, and peptide glycation factor constituted 607 items in total, which we cross-correlated to generate a matrix of 183,921 correlation coefficients. Unsupervised hierarchical clustering and color-coding the correlation coefficients then generated the global correlation map. We hypothesized that such a map would group the plasma proteome in such a way that proteins and clinical parameters associated with the same underlying regulatory mechanism would cluster in the same area. Thus, the global correlation map would both capture large-scale organizational features of the plasma proteome as well as individual associations between proteins and connect them to measures of disease state represented by clinical parameters.

A wealth of information can be found in the correlation map (Figure 3A), with co-regulated areas as large as 76 × 76 items and as small as binary associations. For functional interpretation, we employed bioinformatic keyword annotation and subsequent Fisher's exact tests. The largest structure belonged to the innate immune system and was further dominated by a sub-cluster with very strong correlations. A cluster consisting of immunoglobulins was nearly as large as 68 × 68. The global correlation analysis also identified a cluster dominated by HDL but also containing adiponectin (the protein and the clinical parameter), which is positively associated with peripheral insulin sensitivity (Lihn et al., 2005). Out of more than 20 clusters of similar size, one is associated with LDL particles, another with proteins participating in the coagulation cascade such as the von Willebrand factor (vWF) and fibrinogens, and one contains three steroid-binding proteins (PZP, SHBG, and SERPINA6).

The strongly correlated sub-cluster of the inflammation system includes proteins such as CRP, SAA1, and members of the complement cascade. Furthermore, it contains diabetes-associated clinical parameters such as insulin levels, C-peptide levels, and HOMA-IR, which reflects insulin resistance (Figure 3A). The fact that these disease markers correlate directly within the group of inflammation proteins reflects a link between insulin resistance and systemic inflammation, which is the subject of extensive metabolic research (Moran et al., 2005; Ndumele et al., 2006). Notably, there are also anti-correlating clusters, characterized by off-diagonal areas in the global correlation map (Figure 3A, blue patterns). The main clusters contain inflammation-associated proteins, apolipoproteins, and insulin-sensitivity parameters. For instance, there is a negative correlation between CRP and adiponectin of −0.35, highlighting direct protein-based connections between decreased inflammatory status and increased insulin sensitivity.

Clearly, the global correlation map contains a treasure trove of information about the plasma proteome, encoded in its almost 200,000 correlations. Co-regulated proteins identify proteins associated with diverse physiological processes. Apart from the most apparent functional associations, there are many clusters with no significant keywords as well as many novel connections within the clusters.

Interestingly, some clusters contained information about the sample analysis procedure. These included a tightly co-regulated group of platelet proteins. Although they accurately report on sample quality, they do not reflect intrinsic plasma proteome properties and were therefore removed from downstream analysis (STAR Methods).

To explore the connections between plasma proteins in a complementary way, we generated a network in which the connections are given by their correlation coefficients. For all proteins and clinical parameters in the 20 clusters with the highest number of nodes, we only selected proteins with correlation coefficients of at least 0.4 to display their relationship within and between these clusters (Figure 3B). This highlights the connections within main physiological processes. In the inflammation cluster, for instance, there are strong relationships of the complement system to other inflammatory proteins such as LBP. The network clearly captures the relationship of inflammation, insulin resistance, and lipid metabolism.

RYGB and the Response to Low-Grade Inflammation

Inflammation-associated proteins were found in the largest co-regulated cluster, and they also contained the most highly regulated ones after RYGB (Figures 2 and 4). The connection of obesity, metabolic diseases, and systemic inflammation has been investigated extensively on the molecular and cellular level (Brestoff and Artis, 2015; Osborn and Olefsky, 2012; Quante et al., 2015). Plasma proteome profiling of a cohort of morbidly obese individuals undergoing surgical intervention followed by strong weight loss presents a unique opportunity to investigate changes in the inflammatory response in a systems-wide and unbiased manner. In contrast to previous candidate-driven approaches, our strategy can in principle retrieve association of any plasma protein with weight-related inflammation. To define an inflammatory panel in an unbiased manner, we filtered for relevant keywords (STAR Methods). This resulted in 51 proteins that covered the major pathways, such as complement activation and acute phase reaction. This inflammatory panel was quantified with high consistency in the dataset (90% valid values). We combined the changes of these proteins, normalized to their starting level, into a single value by taking the median, which represents a robust and accurate reflection of the global inflammation status of each individual at each time point. Then, we aggregated the inflammatory status of all participants over time. The longitudinal trajectory of this inflammation status had a maximum at the first post-operative time point with an average increase of 10% (Figure 4A), presumably as a direct consequence of the surgery (Finnerty et al., 2013). Following this brief increase, the global inflammation panel decreased gradually, reaching baseline level 12 weeks after RYGB surgery and the minimum of −11% at the final time point (>104 weeks). This dynamic regulation was quite consistent across almost all participants in the study cohort (Figure S3A).

Proteins included in our inflammation panel were selected by keyword annotation, which could be spurious, including proteins with negative correlation to inflammation. To assess their suitability as markers, we inspected their dynamics and found that the large majority went up at the immediate post-operative time point and stabilized at lower levels at 52 and greater than 104 weeks (Figure 4A). Next, we compared our data to a plasma proteomic profiling study where weight loss was induced by caloric restriction (Cambridge diet), in which 43 participants lost on average 12% of their body mass during an 8-week period and maintained their weight for 1 year (Iepsen et al., 2015). From

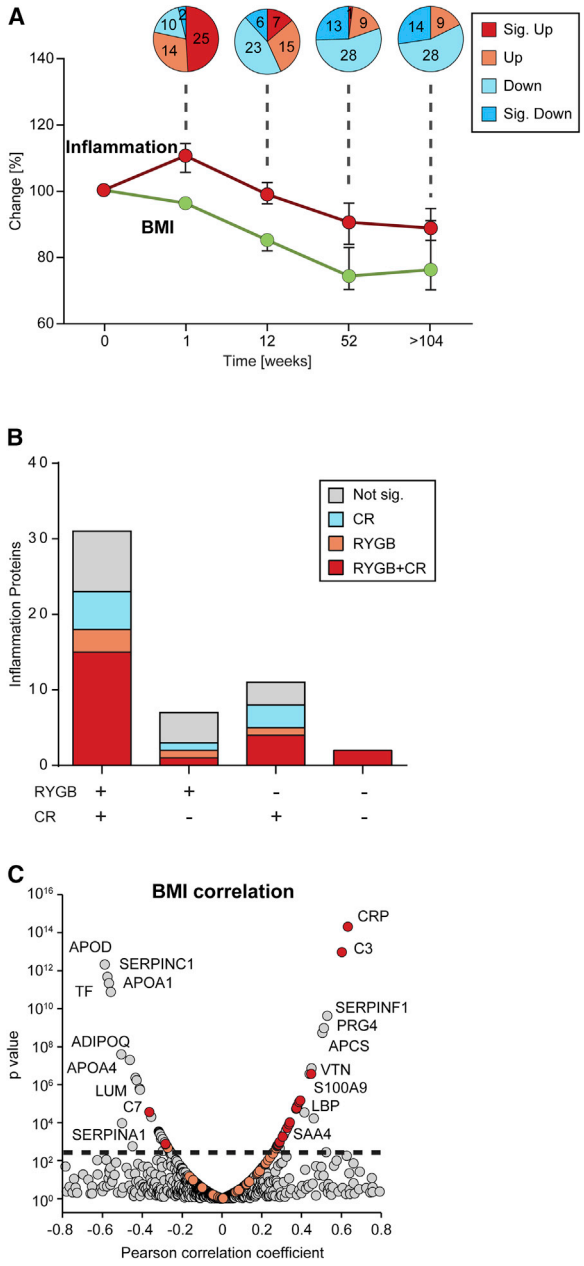

Figure 4. Connection between Global Inflammation Status and Body Mass

(A) Changes of the global inflammation status of all study participants. The global inflammation status is calculated as the median of 51 inflammation proteins, selected by keyword annotation. Pie charts over each of the post-operation time points show the number of proteins, which were up- or downregulated.

(B) Overlap of inflammation proteins in the caloric restriction (CR) and the RYGB studies. Plus and minus indicate if a protein was decreased in both or in one of the two studies. The color code shows how many of the proteins were significantly regulated.

(C) Correlation plot of protein intensities with the BMI in the RYGB study. Inflammation proteins are highlighted in red or orange if they were significantly or not significantly correlated to the BMI, respectively. All proteins above the dashed line show significant correlations.

that study, we had already defined a ten protein inflammation panel (Geyer et al., 2016b), which was completely contained in the current one. After exclusion of the first post-operative time point in the RYGB study, we calculated the slope of the inflammation proteins in both studies across all time points (Table S5). Between caloric restriction achieved through the Cambridge diet and by RYGB surgery, there was an overlap in 31 increased inflammation proteins. Thus, the direction of changes in the full 51 panel in the previous study generally agreed with the current one (Figure 4B). CRP, a prominent risk factor for cardiovascular disease, showed the strongest response, and its levels increased 5-fold at the 1-week time point and decreased 14-fold afterwards.

For further insights into the connection of the plasma proteome to weight loss, we correlated all 1,700 quantified plasma proteins directly to BMI. In total, 51 proteins had a significant correlation, of which 18 were part of our inflammation panel (Figure S3B; Table S6). CRP, complement factor C3, and S100A8 were the proteins with the strongest correlation (Pearson correlation of 0.63, 0.61, and 0.45, respectively). Together with the fact that the BMI clustered with inflammation-annotated proteins in the global correlation map, this underlines the strong connection between inflammation and obesity.

Core Proteins in Lipid Metabolism Are Significantly Altered by RYGB

Lipid homeostasis was the second most strongly affected physiological system by RYGB, and it clustered into two distinct regions of the global correlation map (Figure 2). Many of the proteins found in this cluster are well-known constituents of different lipoprotein particles such as APOB or receptors of these particles such as the LDL receptor (LDLR). To elucidate their behavior, we filtered the identified plasma proteome for the Gene Ontology cellular compartment (GOCC) terms "lipid transport," "chylomicron," "high density lipoprotein (HDL)," "low density lipoprotein (LDL)," "intermediate density lipoprotein (IDL)," and "very low density lipoprotein (vLDL)" particle. To this set, we added non-annotated proteins well known to be associated with lipid metabolism such as apolipoprotein D (APOD), apolipoprotein(a) (LPA), Prolow-density lipoprotein receptor-related protein 1 (LRP1), and phospholipid transfer protein (PLTP). Excluding the keyword-annotated inflammation proteins SAA1, SAA2, and SAA4 resulted in 25 proteins that reflect the lipid homeostasis system in blood. They were consistently quantified across all patients and time points. Furthermore, their correlation map reveals a large degree of similarity between the caloric restriction and RYGB studies (Figures 5A and 5B). For instance, the highly correlated clusters for apolipoproteins APOC1, APOC2, APOC3, APOC4, and APOE, which are LDL constituents, are almost superimposable. Likewise, the HDL related proteins — APOA1, APOA2, APOA4, and PON1 — correlated highly.

Inspecting the direction of changes in the expression levels of proteins, we found that the HDL constituents APOA1, APOA2, APOA4, and PON1 increased in RYGB but decreased in caloric restriction, reflecting the HDL laboratory values that were measured independently in these studies (Figure S4). Furthermore, HDL-associated proteins such as APOC1, APOC2, APOC4, APOM, PLTP, LPA, and several others that may be

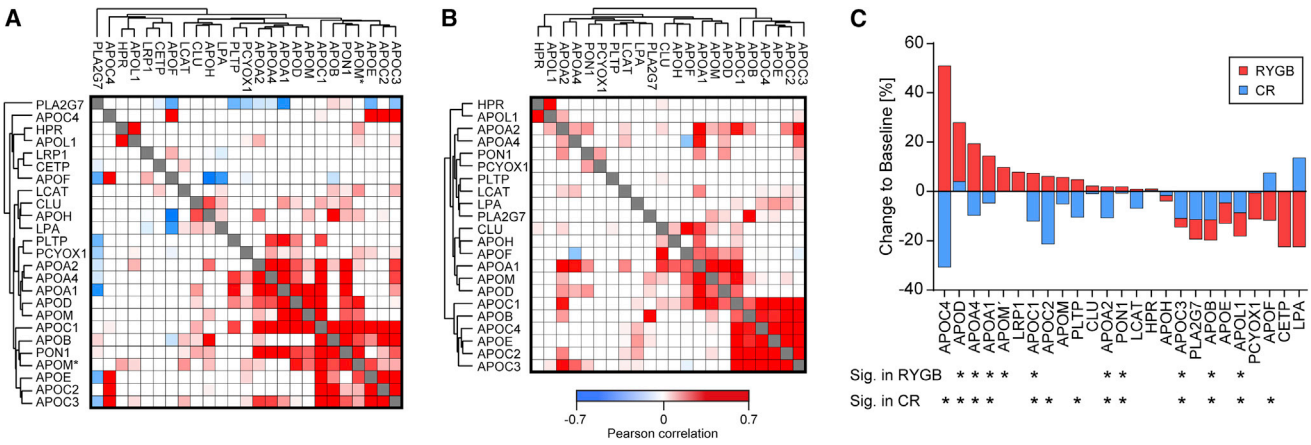

Figure 5. Response of Lipid Homeostasis Regulating Proteins to RYGB and Caloric Restriction

(A) Correlation maps of lipid homeostasis-associated proteins in the RYGB study.

(B) Correlation maps of lipid homeostasis-associated proteins in the caloric restriction study.

(C) Median of protein intensities showing increased or decreased expression after RYGB and caloric restriction (CR). Significantly changed proteins are marked with an asterisk.

associated were regulated in opposite directions. One of those — APOC1 — has broad physiological functions including inhibition of fatty acid uptake from adipocytes and inhibition of lipoprotein binding to LDL. Interestingly, APOC1 was a member of both the LDL and HDL correlation clusters. In caloric restriction, its levels decreased by 12%, whereas in RYGB they increased by 7%. This could be due to a lower need for transport of fatty acids after caloric restriction but not after RYGB and may reflect the mechanistic differences of these two weight loss interventions. Interestingly, mice overexpressing APOC1 seem protected for obesity and insulin resistance due to reduced fatty acid uptake in adipocytes (Jong et al., 2001).

After RYGB, insulin sensitivity of the liver rapidly improves (Bojsen-Møller et al., 2014). In line with this, we observed increases in APOA4, another surrogate marker of hepatic insulin sensitivity (VerHague et al., 2013).

Improvement in Insulin Sensitivity after RYGB Is Reflected in the Plasma Proteome

The immediate positive effect of RYGB on insulin sensitivity has been widely discussed, but any reflections of this in the plasma proteome have not been described. In both RYGB cohorts, we determined hepatic insulin resistance by the HOMA-IR based on C-peptide, and, in study 1, we further measured "hepatic insulin sensitivity" by tracer estimation of hepatic glucose production, "peripheral insulin sensitivity" by the hyperinsulinemic euglycemic clamp and "oral glucose insulin sensitivity" from oral glucose tolerance test, resulting in a system-wide assessment of insulin sensitivity (Figure S5).

Connecting the insulin sensitivity measures to the plasma proteome profile retrieved 75 significantly correlating proteins (Figures 6A and 6B; Table S7). Adiponectin, sex hormone-binding globulin, vitamin K-dependent protein S, cholinesterase, the complement factors C3, CFB, and C4-binding protein alpha chain correlated with all four assessments. We calculated a summed insulin sensitivity correlation, taking the strength and number of correlations into account and followed this measure over time since surgery (Figure 6C; Table S8). This factor reached its maximum 1 year after the gastric bypass operation. Interestingly, the summed insulin sensitivity correlation was almost superimposed in both studies (Figure 6B), validating the individual correlating proteins.

Reassuringly, adiponectin, a classical marker for insulin sensitivity, was the protein with the highest score (ADIPOQ; S:16), and sex hormone-binding globulin (SHBG; S:8) and complement factor C3 (C3; S:8) were likewise in the top group. Strikingly, another 25 proteins and the "peptide glycation" factor correlated or anti-correlated highly with insulin sensitivity (Figure 6A). Other proteins in this heterogeneous group included pigment epithelium-derived factor (SERPINF1; S:11), afamin (AFM; S:10), antithrombin-III (SERPINC1; S:9), and apolipoprotein A1 (APOA1; S:8). Note that some of these correlations may simply reflect the weight loss, rather than a more specific effect on insulin sensitivity. For instance, SERPINF1, a protein secreted by adipocytes, is clearly and highly significantly anti-correlated to insulin sensitivity — especially to hepatic insulin sensitivity (Pearson's R -0.66; $p < 10^{-9}$). Of note, we had previously found a strong association of SERPINF1 and weight loss in the caloric restriction study as well as a correlation to insulin resistance based on HOMA-IR (Geyer et al., 2016b). It would be interesting to determine if SERPINF1 has a functional involvement in insulin sensitivity or if it mainly reflects total fat mass.

Conversely, a group of high-scoring proteins reflecting the inflammatory state and lipid transport likely represent functional connections: both systemic inflammation and dysregulated lipid homeostasis. These included several components of the complement system and a number of apolipoproteins, which also correlated or anti-correlated with insulin sensitivity measures in our global correlation map (Figure 3; Table S8). Clearly, our protein correlation profiles reflect the complex relationships between insulin sensitivity, lipid homeostasis, and inflammation. However, the majority of proteins correlated with insulin sensitivity had no reported connection to these two physiological

A

	Hepatic insulin sensitivity	HOMA-IR	Peripheral insulin sensitivity	Oral glucose insulin sensitivity	Total Score
ADIPOQ	0.61	-0.50	0.71	0.61	16
SERPINF1	-0.66	0.41	-0.50	---	11
AFM	-0.43	0.43	---	-0.57	10
CFH	-0.35	0.39	-0.39	-0.52	9
SHBG	0.38	-0.37	0.48	0.49	9
C3	-0.39	0.44	-0.38	-0.46	9
SERPINC1	0.46	-0.44	0.40	---	9
C4BPA	-0.36	0.38	-0.37	-0.52	8
PROS1	-0.34	0.23	-0.43	-0.51	8
BCHE	-0.51	0.22	-0.42	-0.38	8
APOA1	0.45	-0.43	0.36	---	8
TF	0.40	-0.39	0.49	---	7
APCS	-0.39	0.41	---	-0.42	6
CPN1	-0.43	---	-0.42	-0.37	6
MANBA	0.44	---	0.49	---	6
ITIH3	0.44	-0.24	0.38	---	6
APOD	0.46	-0.42	---	---	6
APOC1	0.52	-0.37	---	---	6
CNDP1	-0.42	0.32	---	-0.47	5
HBA1;HBA2	-0.43	---	-0.43	---	5
PRG4	-0.42	0.41	-0.37	---	5
C8B	---	0.26	---	-0.49	4
FCN3	-0.37	0.26	---	-0.47	4
CFI	-0.34	0.32	---	-0.41	4
VCAN	---	---	---	0.54	4
Peptide Glycation	---	0.41	---	-0.38	4
A1BG	---	-0.23	0.42	---	4
C8G	-0.49	0.29	---	---	4
CFHR5	0.54	---	---	---	4

B

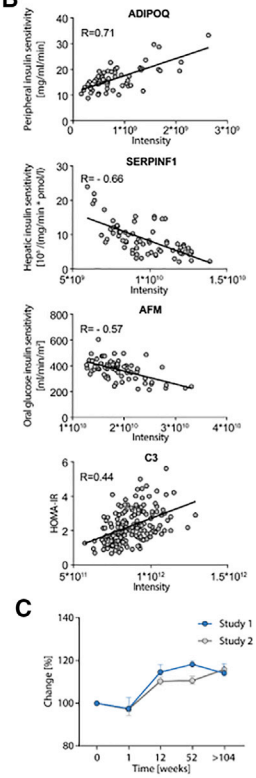

C

Figure 6. Correlation to Insulin Sensitivity Assessments

(A) Correlation of the plasma proteome profile to the four insulin sensitivity assessments: hepatic insulin sensitivity, homeostatic model assessment of insulin resistance based on C-peptide (HOMA-IR), peripheral insulin sensitivity, and oral glucose insulin sensitivity. Pearson correlations were rank-ordered, and proteins grouped, scored, and color-coded from 1 to 4.

(B) Example correlations of four proteins to the insulin sensitivity assessments.

(C) Trajectories of the summed insulin sensitivity correlations defined in (A) over time. Blue, RYGB study 1; gray, RYGB study 2.

processes. As insulin has a broad effect on different organs, it is not surprising that proteins of different physiological processes correlated to insulin sensitivity, which makes them interesting candidates to study as cause or consequence of insulin resistance.

DISCUSSION

Bariatric surgery fundamentally alters human metabolism, and much remains to be learned about the molecular mechanisms underlying surgical therapies such as RYGB. The majority of research has focused on anthropometric as well as clinical and physiological data (Puzziferri et al., 2014), whereas there are few hypothesis-free approaches (Arora et al., 2015; Luo et al., 2016). In this work, we aimed to describe global rearrangements of the plasma proteome in a systems-wide view and discover protein markers of gastric bypass surgery with possible functional relevance. This was enabled by a recently developed robust and highly reproducible pipeline for MS-based investigation of plasma, which we termed plasma proteome profiling (Geyer et al., 2016a). In the current study, we integrated several technological advances into the workflow including the spider fractionator to generate deep peptide libraries and combined it for the first time with the BoxCar scan method to increase the dynamic range of our measurements (Meier et al., 2018). Together, this achieved the most extensive quantitative plasma proteome so far, providing the community with concentration estimates of over 1,700 proteins and their bioinformatic keyword annotations.

We described longitudinal trajectories of 114 significantly altered proteins in response to RYGB and applied functional annotation analysis to reveal the underlying physiological mechanisms. This identified two main groups, belonging to the inflammation and the lipid homeostasis systems. We found a strong overlap of inflammation proteins in RYGB with our previous study on caloric restriction-induced weight loss (Geyer et al., 2016b) with the same regulation and tight correlation to BMI. We conclude that body mass is a major determinant of systemic low-grade inflammation levels and that weight loss — regardless of the mode by which it is achieved — is its most important driver. These dramatic changes are illustrated by regulation of 51 inflammation-associated proteins, the most prominent of which is CRP that decreased 14-fold during the average weight reduction of 28%. Note that a few of these proteins were upregulated, for instance, the complement factor C7. Interestingly, our unbiased analysis revealed that the weight loss-driven decrease over the subsequent year was as strong as the immediate surgery-induced increase. Such dramatic changes in systematic

inflammation could affect the risk for cardiovascular events (Danesh et al., 2000).

In contrast to the inflammation system, the lipid homeostasis system was differently regulated between caloric restriction and RYGB. While LDL-associated proteins decreased in both interventions, the HDL-associated cluster was only increased after RYGB. This is interesting given the link between high HDL levels and a lower risk of coronary heart disease in associative studies but not when increased by pharmacological intervention (Rader and Hovingh, 2014). At this point, the majority of differently regulated proteins between both types of weight loss cannot be directly linked to clinically measured HDL levels alone.

Lipoprotein particles can be sub-classified into several types that interact or are converted into each other (Kontush et al., 2013). Proteins are the defining elements of all of them and could be the basis for more rational classification of the lipid homeostasis system. In our study, several cardiovascular risk markers from the lipid homeostasis system such as the LDL-associated APOB and LPA dropped in both caloric restriction and RYGB, whereas APOA1, whose levels positively correlate with decreased cardiovascular risk (Emerging Risk Factors Collaboration et al., 2012), significantly increased only in RYGB. A number of such factors emerged from our analyses (Table S9), and it would be interesting to study them in-depth for a possible differential involvement in cardiovascular diseases. More generally, it has been widely discussed which types of cholesterol particles are the most relevant to disease risk (Krauss, 2010), and our data now suggest that it may be promising to focus on the different lipoprotein-associated proteins themselves (Hegele, 2009). For the future, we imagine that plasma proteome profiling of cardiovascular risk studies may help to unravel the role and biomarker potential of individual proteins.

The plasma proteome profiles of a well-characterized longitudinal cohort with comprehensive clinical characterization provided the first opportunity to systematically study the dynamics of the human plasma proteome. For this purpose, we here employed global correlation maps, in which we correlated the quantitative levels of all proteins and clinical parameters to each other. We sorted the resulting matrix by hierarchical clustering and applied bioinformatic enrichment analysis. This disentangled complex processes in the plasma proteome and associated proteins to common physiological functions and clinical risk measures.

Standard clinical parameters for insulin resistance including insulin levels themselves, C-peptide levels, and HOMA-IR, clustered with proteins of the inflammation system. Hepatic insulin sensitivity, peripheral insulin sensitivity, and oral glucose insulin sensitivity all tended to associate with proteins of the lipid homeostasis system. Network analysis highlighted an anti-correlation between those two systems (Figure 3B). This is consistent with the detrimental effect of systemic inflammation on the risk of metabolic disease and the positive and negative effects of the levels of different cholesterol lipoprotein particles (Dali-Youcef et al., 2013; Glass and Olefsky, 2012). Thus, we here recapitulated the relationships between insulin sensitivity, the lipid homeostasis system, and systemic inflammation purely from an unbiased assessment of the plasma proteome in a human intervention study for diabetes. Interestingly, our analysis revealed that known single protein markers of insulin sensitivity, such as adiponectin (Li et al., 2009), were indeed the highest scoring ones, and that there are many others that have not yet been connected to insulin sensitivity (Figure 6; Table S8).

In conclusion, plasma proteome profiling is a powerful technology for studying the effects of physiological interventions such as RYGB in humans, which may provide new molecular markers and targets for the treatment of metabolic syndrome and diabetes. The approach can assess changes in circulating proteins resulting from any metabolic perturbation. Our bioinformatic analysis integrates these data with existing knowledge, thereby providing a functional and clinical context for interpretation. Further streamlining of the analytical methods developed here will make it possible to measure many clinical studies, building up a comprehensive "knowledge base" of the human plasma proteome in health and disease states (Geyer et al., 2017).

STAR★METHODS

Detailed methods are provided in the online version of this paper and include the following:

- KEY RESOURCES TABLE
- CONTACT FOR REAGENT AND RESOURCE SHARING
- EXPERIMENTAL MODEL AND SUBJECT DETAILS
- METHOD DETAILS
  - High Abundant Protein Depletion for Building a Matching Library
  - Sample Preparation for Study Samples
  - High Pressure Liquid Chromatography and Mass Spectrometry
  - Data Analysis
- QUANTIFICATION AND STATISTICAL ANALYSIS
  - Global Correlation Analysis
  - Inflammation System
  - Lipid Homeostasis System
  - Scoring System for Insulin Sensitivity
  - Insulin Sensitivity Score
- DATA AND SOFTWARE AVAILABILITY

SUPPLEMENTAL INFORMATION

Supplemental Information includes five figures and nine tables and can be found with this article online at https://doi.org/10.1016/j.cels.2018.10.012.

ACKNOWLEDGMENTS

We thank all members of the Proteomics and Signal Transduction group (Max-Planck Institute) and the Clinical Proteomics group (NNF Center for Protein Research) and in particular, Atul Deshmuk, for their help and discussions. In addition, we thank Igor Paron, Christian Deiml, Korbinian Mayr, Gaby Sowa, and Katharina Zettl for technical assistance; and Jürgen Cox for bioinformatic tools.

The work carried out in this project was partially supported by the Max Planck Society for the Advancement of Science, the European Union's Horizon 2020 research and innovation program (grant agreement no. 686547; MSmed project), the European Commission 7th Research Framework Program (GA ERC-2012-SyG_318987; ToPAG project), and by the Novo Nordisk Foundation for the Clinical Proteomics group (grant NNF15CC0001).

AUTHOR CONTRIBUTIONS

N.J.W.A. and P.E.G. designed, performed, and interpreted the MS-based proteomic analysis of patient plasma and wrote the paper and generated the figures. S.D., P.V.T., F.M., L.N., A.S., and E.C.K. interpreted proteomic data and revised the manuscript. K.N.B.-M., N.B.J., C.M., S.M., J.J.H., and S.S.T. provided patient material and clinical data and revised the manuscript. M.M. designed and interpreted the MS-based proteomic analysis of patient plasma, supervised and guided the project, and wrote the paper.

DECLARATION OF INTERESTS

The authors declare no competing interests.

Received: April 20, 2018
Revised: September 10, 2018
Accepted: October 25, 2018
Published: December 5, 2018

REFERENCES

Aab, A., Abreu, P., Aglietta, M., Ahn, E.J., Al Samarai, I., Albuquerque, I.F., Allekotte, I., Allison, P., Almela, A., Alvarez Castillo, J., et al. (2016). Measurement of the radiation energy in the radio signal of extensive air showers as a universal estimator of cosmic-ray energy. Phys. Rev. Lett. *116*, 241101.

Adams, T.D., Davidson, L.E., Litwin, S.E., Kim, J., Kolotkin, R.L., Nanjee, M.N., Gutierrez, J.M., Frogley, S.J., Ibele, A.R., Brinton, E.A., et al. (2017). Weight and metabolic outcomes 12 years after gastric bypass. N. Engl. J. Med. *377*, 1143–1155.

Aebersold, R., and Mann, M. (2016). Mass-spectrometric exploration of proteome structure and function. Nature *537*, 347–355.

Arora, T., Velagapudi, V., Pournaras, D.J., Welbourn, R., le Roux, C.W., Orešič, M., and Bäckhed, F. (2015). Roux-en-Y gastric bypass surgery induces early plasma metabolomic and lipidomic alterations in humans associated with diabetes remission. PLoS One *10*, e0126401.

Bojsen-Møller, K.N., Dirksen, C., Jørgensen, N.B., Jacobsen, S.H., Serup, A.K., Albers, P.H., Hansen, D.L., Worm, D., Naver, L., Kristiansen, V.B., et al. (2014). Early enhancements of hepatic and later of peripheral insulin sensitivity combined with increased postprandial insulin secretion contribute to improved glycemic control after Roux-en-Y gastric bypass. Diabetes *63*, 1725–1737.

Bojsen-Møller, K.N., Dirksen, C., Svane, M.S., Jørgensen, N.B., Holst, J.J., Richter, E.A., and Madsbad, S. (2017). Variable reliability of surrogate measures of insulin sensitivity after Roux-en-Y gastric bypass. Am. J. Physiol. Regul. Integr. Comp. Physiol. *312*, R797–R805.

Brestoff, J.R., and Artis, D. (2015). Immune regulation of metabolic homeostasis in health and disease. Cell *161*, 146–160.

Cardoso, L., Rodrigues, D., Gomes, L., and Carrilho, F. (2017). Short- and long-term mortality after bariatric surgery: a systematic review and meta-analysis. Diabetes Obes. Metab. *19*, 1223–1232.

Cox, J., Hein, M.Y., Luber, C.A., Paron, I., Nagaraj, N., and Mann, M. (2014). Accurate proteome-wide label-free quantification by delayed normalization and maximal peptide ratio extraction, termed MaxLFQ. Mol. Cell. Proteomics *13*, 2513–2526.

Cox, J., and Mann, M. (2008). MaxQuant enables high peptide identification rates, individualized p.p.b.-range mass accuracies and proteome-wide protein quantification. Nat. Biotechnol. *26*, 1367–1372.

Cox, J., Neuhauser, N., Michalski, A., Scheltema, R.A., Olsen, J.V., and Mann, M. (2011). Andromeda: a peptide search engine integrated into the MaxQuant environment. J. Proteome Res. *10*, 1794–1805.

Cummings, D.E., and Rubino, F. (2018). Metabolic surgery for the treatment of type 2 diabetes in obese individuals. Diabetologia *61*, 257–264.

Dali-Youcef, N., Mecili, M., Ricci, R., and Andrès, E. (2013). Metabolic inflammation: connecting obesity and insulin resistance. Ann. Med. *45*, 242–253.

Danesh, J., Whincup, P., Walker, M., Lennon, L., Thomson, A., Appleby, P., Gallimore, J.R., and Pepys, M.B. (2000). Low grade inflammation and coronary heart disease: prospective study and updated meta-analyses. BMJ *321*, 199–204.

Emerging Risk Factors Collaboration, Di Angelantonio, E., Gao, P., Pennells, L., Kaptoge, S., Caslake, M., Thompson, A., Butterworth, A.S., Sarwar, N., Wormser, D., et al. (2012). Lipid-related markers and cardiovascular disease prediction. JAMA *307*, 2499–2506.

Finnerty, C.C., Mabvuure, N.T., Ali, A., Kozar, R.A., and Herndon, D.N. (2013). The surgically induced stress response. JPEN J. Parenter. Enteral Nutr. *37*, 21S–29S.

GBD 2015 Obesity Collaborators, Afshin, A., Forouzanfar, M.H., Reitsma, M.B., Sur, P., Estep, K., Lee, A., Marczak, L., Mokdad, A.H., Moradi-Lakeh, M., et al. (2017). Health effects of overweight and obesity in 195 countries over 25 years. N. Engl. J. Med. *377*, 13–27.

Geyer, P.E., Holdt, L.M., Teupser, D., and Mann, M. (2017). Revisiting biomarker discovery by plasma proteomics. Mol. Syst. Biol. *13*, 942.

Geyer, P.E., Kulak, N.A., Pichler, G., Holdt, L.M., Teupser, D., and Mann, M. (2016a). Plasma proteome profiling to assess human health and disease. Cell Syst. *2*, 185–195.

Geyer, P.E., Wewer Albrechtsen, N.J., Tyanova, S., Grassl, N., Iepsen, E.W., Lundgren, J., Madsbad, S., Holst, J.J., Torekov, S.S., and Mann, M. (2016b). Proteomics reveals the effects of sustained weight loss on the human plasma proteome. Mol. Syst. Biol. *12*, 901.

Glass, C.K., and Olefsky, J.M. (2012). Inflammation and lipid signaling in the etiology of insulin resistance. Cell Metab. *15*, 635–645.

Griffen, W.O., Jr., Young, V.L., and Stevenson, C.C. (1977). A prospective comparison of gastric and jejunoileal bypass procedures for morbid obesity. Ann. Surg. *186*, 500–509.

Hegele, R.A. (2009). Plasma lipoproteins: genetic influences and clinical implications. Nat. Rev. Genet. *10*, 109–121.

Iepsen, E.W., Lundgren, J., Dirksen, C., Jensen, J.E., Pedersen, O., Hansen, T., Madsbad, S., Holst, J.J., and Torekov, S.S. (2015). Treatment with a GLP-1 receptor agonist diminishes the decrease in free plasma leptin during maintenance of weight loss. Int. J. Obes. (Lond.) *39*, 834–841.

Jong, M.C., Voshol, P.J., Muurling, M., Dahlmans, V.E., Romijn, J.A., Pijl, H., and Havekes, L.M. (2001). Protection from obesity and insulin resistance in mice overexpressing human apolipoprotein C1. Diabetes *50*, 2779–2785.

Keilhauer, E.C., Geyer, P.E., and Mann, M. (2016). HCD fragmentation of glycated peptides. J. Proteome Res. *15*, 2881–2890.

Kontush, A., Lhomme, M., and Chapman, M.J. (2013). Unraveling the complexities of the HDL lipidome. J. Lipid Res. *54*, 2950–2963.

Krauss, R.M. (2010). Lipoprotein subfractions and cardiovascular disease risk. Curr. Opin. Lipidol. *21*, 305–311.

Kulak, N.A., Geyer, P.E., and Mann, M. (2017). Loss-less nano-fractionator for high sensitivity, high coverage proteomics. Mol. Cell. Proteomics *16*, 694–705.

Li, S., Shin, H.J., Ding, E.L., and van Dam, R.M. (2009). Adiponectin levels and risk of type 2 diabetes: a systematic review and meta-analysis. JAMA *302*, 179–188.

Lihn, A.S., Pedersen, S.B., and Richelsen, B. (2005). Adiponectin: action, regulation and association to insulin sensitivity. Obes. Rev. *6*, 13–21.

Luo, P., Yu, H., Zhao, X., Bao, Y., Hong, C.S., Zhang, P., Tu, Y., Yin, P., Gao, P., Wei, L., et al. (2016). Metabolomics study of Roux-en-Y gastric bypass surgery (RYGB) to treat type 2 diabetes patients based on ultraperformance liquid chromatography-mass spectrometry. J. Proteome Res. *15*, 1288–1299.

Madsbad, S., and Holst, J.J. (2014). GLP-1 as a mediator in the remission of type 2 diabetes after gastric bypass and sleeve gastrectomy surgery. Diabetes *63*, 3172–3174.

Martinussen, C., Bojsen-Møller, K.N., Dirksen, C., Jacobsen, S.H., Jørgensen, N.B., Kristiansen, V.B., Holst, J.J., and Madsbad, S. (2015). Immediate enhancement of first-phase insulin secretion and unchanged glucose effectiveness in patients with type 2 diabetes after Roux-en-Y gastric bypass. Am. J. Physiol. Endocrinol. Metab. *308*, E535–E544.

Mason, E.E., and Ito, C. (1967). Gastric bypass in obesity. Surg. Clin. North Am. *47*, 1345–1351.

Mason, E.E., Printen, K.J., Hartford, C.E., and Boyd, W.C. (1975). Optimizing results of gastric bypass. Ann. Surg. *182*, 405–414.

Meier, F., Geyer, P.E., Virreira Winter, S., Cox, J., and Mann, M. (2018). BoxCar acquisition method enables single-shot proteomics at a depth of 10,000 proteins in 100 minutes. Nat. Methods *15*, 440–448.

Miras, A.D., and le Roux, C.W. (2013). Mechanisms underlying weight loss after bariatric surgery. Nat. Rev. Gastroenterol. Hepatol. *10*, 575–584.

Moran, A., Steffen, L.M., Jacobs, D.R., Jr., Steinberger, J., Pankow, J.S., Hong, C.P., Tracy, R.P., and Sinaiko, A.R. (2005). Relation of C-reactive protein to insulin resistance and cardiovascular risk factors in youth. Diabetes Care *28*, 1763–1768.

Nagaraj, N., Kulak, N.A., Cox, J., Neuhauser, N., Mayr, K., Hoerning, O., Vorm, O., and Mann, M. (2012). System-wide perturbation analysis with nearly complete coverage of the yeast proteome by single-shot ultra HPLC runs on a bench top Orbitrap. Mol. Cell. Proteomics *11*, M111.013722.

Ndumele, C.E., Pradhan, A.D., and Ridker, P.M. (2006). Interrelationships between inflammation, C-reactive protein, and insulin resistance. J. Cardiometab. Syndr. *1*, 190–196.

Osborn, O., and Olefsky, J.M. (2012). The cellular and signaling networks linking the immune system and metabolism in disease. Nat. Med. *18*, 363–374.

Puzziferri, N., Roshek, T.B., 3rd, Mayo, H.G., Gallagher, R., Belle, S.H., and Livingston, E.H. (2014). Long-term follow-up after bariatric surgery: a systematic review. JAMA *312*, 934–942.

Quante, M., Dietrich, A., ElKhal, A., and Tullius, S.G. (2015). Obesity-related immune responses and their impact on surgical outcomes. Int. J. Obes. (Lond.) *39*, 877–883.

Rader, D.J., and Hovingh, G.K. (2014). HDL and cardiovascular disease. Lancet *384*, 618–625.

Sjöström, L., Narbro, K., Sjöström, C.D., Karason, K., Larsson, B., Wedel, H., Lystig, T., Sullivan, M., Bouchard, C., Carlsson, B., et al. (2007). Effects of bariatric surgery on mortality in Swedish obese subjects. N. Engl. J. Med. *357*, 741–752.

Tyanova, S., Temu, T., Sinitcyn, P., Carlson, A., Hein, M.Y., Geiger, T., Mann, M., and Cox, J. (2016). The Perseus computational platform for comprehensive analysis of (prote)omics data. Nat. Methods *13*, 731–740.

VerHague, M.A., Cheng, D., Weinberg, R.B., and Shelness, G.S. (2013). Apolipoprotein A-IV expression in mouse liver enhances triglyceride secretion and reduces hepatic lipid content by promoting very low density lipoprotein particle expansion. Arterioscler. Thromb. Vasc. Biol. *33*, 2501–2508.

W.H.O. (2016). Global Health Observatory (GHO) data. Overweight and obesity. http://www.who.int/gho/ncd/risk_factors/overweight/en/.

Wittgrove, A.C., Clark, G.W., and Tremblay, L.J. (1994). Laparoscopic gastric bypass, Roux-en-Y: preliminary report of five cases. Obes. Surg. *4*, 353–357.

Worm, D., Madsbad, S., Kristiansen, V.B., Naver, L., and Hansen, D.L. (2015). Changes in hematology and calcium metabolism after gastric bypass surgery–a 2-year follow-up study. Obes. Surg. *25*, 1647–1652.

STAR★METHODS

KEY RESOURCES TABLE

REAGENT or RESOURCE	SOURCE	IDENTIFIER
Biological Samples		
RYGB study 1	Bojsen-Møller et al. (2014)	Clinical trial NCT01202526
RYGB study 2	Martinussen et al. (2015)	Clinical trial NCT01993511
Chemicals, Peptides, and Recombinant Proteins		
Multiple Affinity Removal Spin Cartridge Human 6	Agilent Technologies	Cat#5188-5230
High Select™ Top14 Abundant Protein Depletion Midi Spin Column	Thermo Fisher Scientific	Cat#A36371
'iST' Kit for proteomic sample preparation	PreOmics GmbH	P.O. 00001
Deposited Data		
Proteomics data	PRIDE ProteomeXchange	PXD009348
Software and Algorithms		
MaxQuant	Cox and Mann (2008)	Version 1.5.9.4
Perseus	Tyanova et al. (2016)	Version 1.5.5.5

CONTACT FOR REAGENT AND RESOURCE SHARING

Further information and requests for resources and reagents should be directed to and will be fulfilled by the Lead Contact, Matthias Mann (mmann@biochem.mpg.de).

EXPERIMENTAL MODEL AND SUBJECT DETAILS

RYGB study 1: Ten obese patients with type 2 diabetes (age 43.6 ± 3.4 years, male/female 4/6, BMI 38.9 ± 1.6 kg/m^2, HbA1c 7.0 ± 0.3%, diabetes duration 3.3 ± 1.0 years) and ten obese patients with normal glucose tolerance (age 40.1 ± 2.8 years, male/female 3/7, BMI 40.2 ± 0.8 kg/m^2, HbA1c 5.4 ± 0.1%) scheduled for laparoscopic Roux-en-Y gastric bypass (RYGB) were investigated before (n=20), 1 week (n=16), 3 months (n=20) and 1 year (n=18) postoperatively (Clinical trial NCT01202526), as described previously (Bojsen-Møller et al., 2014). At 4 years post-RYGB, an extension study (NCT03046147) was initiated and 16 patients of the initial cohort accepted to be included. Written informed consent was obtained from all participants and the study was approved by the Municipal Ethical Committee of Copenhagen in accordance with the Helsinki declaration and by the Danish Data Protection Agency. Triple sampling at fasting was performed at all study visits, while hyperinsulinemic-euglycemic clamps (HEC) including basal glucose tracer infusions were performed at all except the 4 year's visit as previously described in detail. Oral glucose tolerance tests (OGTTs) were done on separate study days before, 3 months, 1 year and 4 years after RYGB. Antidiabetic agents were discontinued $\geq$3 days before each study day, and participants were instructed to refrain from strenuous physical activity and alcohol for 3 days and to fast overnight (10-12 h) prior to all experiments. Calculations: HOMA2-IR was calculated from all study visits based on a triple sampling of fasting glucose and C-peptide concentrations using the HOMA2. Hepatic insulin sensitivity and peripheral insulin sensitivity were estimated from HEC experimental days as the tracer determined basal rate of appearance (Ra) of glucose (in mg per minute) with correction for C-peptide concentrations and the tracer determined rate of disappearance (Rd) of glucose during the HEC expressed as mg per min per kg fat free mass (ffm), respectively. The Oral Glucose Insulin Sensitivity index was estimated from all OGTTs and has recently been validated against the HEC in this particular cohort (Bojsen-Møller et al., 2017).

RYGB study 2: Participants: Ten obese patients with type 2 diabetes (age 46.1 ± 2.8 years, male/female 4/6, BMI 41.2 ± 1.3 kg/m^2, HbA1c 45.1 ± 2.2 mmol/mol, diabetes duration 3.6 ± 1.3 years), seven obese patients with impaired glucose tolerance (age 41.8 ± 3.7 years, male/female 2/5, BMI 40.3 ± 1.6 kg/m^2, HbA1c 40.0 ± 1.0 mmol/mol) and ten obese patients with normal glucose tolerance (age 41.6 ± 3.0 years, male/female 4/6, BMI 43.8 ± 1.5 kg/m^2, HbA1c 35.0 ± 1.3 mmol/mol) were examined before (n=27) and 1 week (n=25) and 3 months (n=25) after RYGB (NCT01993511) as previously described (Martinussen et al., 2015). A few of the patients were also investigated after 1 year (n=6) and 2 years (n=3) postoperatively. Written informed consent was obtained from all participants and the study was approved by the Municipal Ethical Committee of Copenhagen in accordance with the Helsinki declaration and by the Danish Data Protection Agency. Triple sampling at fasting was performed at all study visits. Oral glucose tolerance testing was done on separate study days before (n=23) and 3 months (n=23) and 1 year (n=5) after RYGB. Antidiabetic medication was discontinued >3 days (>10 days for Liraglutide) prior to surgery and patients were instructed to fast overnight (10-12 hours) prior to testing. Calculations: HOMA2-IR and oral glucose insulin sensitivity was obtained as described for study 1.

METHOD DETAILS

High Abundant Protein Depletion for Building a Matching Library

To construct a library of peptide identifications, we used two commercial depletion kits that together remove the top14 highest abundant proteins in plasma (Geyer et al., 2016a). Following depletion, we separated our samples into 24 fractions, using our recently developed high-pH reversed-phase 'Spider fractionator' (Figure 1B) (Kulak et al., 2017).

Sample Preparation for Study Samples

Plasma samples for the quantitative analysis of the two bariatric surgery cohorts were prepared for all samples according to the previously published Plasma Proteome Profiling pipeline (Geyer et al., 2016a). In brief, this involved optimized conditions for denaturation, alkylation, digestion and peptide purification, and liquid chromatography and MS settings. Sample preparation was carried out in an automated liquid handling platform (Agilent Bravo) in a 96 well format. For sample preparation, we used the 'iST' Kit for proteomic sample preparation (P.O. 00001, PreOmics GmbH). Depletion was only used for the library and not for the study samples.

High Pressure Liquid Chromatography and Mass Spectrometry

Samples were measured using LC-MS instrumentation consisting of an EASY-nLC 1200 system (Thermo Fisher Scientific), which was combined with a Q Exactive HF Orbitrap (Thermo Fisher Scientific) and a nano-electrospray ion source (Thermo Fisher Scientific). Purified peptides were separated on 40 cm HPLC-columns (ID: 75 μm; in-house packed into the tip with ReproSil-Pur C18-AQ 1.9 μm resin (Dr. Maisch GmbH)). For each LC-MS/MS analysis, around 1 μg peptides were used for the 45 min gradients and for the fractions of the deep plasma data set. Peptides were loaded in buffer A (0.1% formic acid, 5% DMSO (v/v)) and eluted with a linear 35 min gradient of 3-30% of buffer B (0.1% formic acid, 5% DMSO, 80% (v/v) acetonitrile), followed by a 7 min increase to 75% of buffer B and a 1 min increase to 98% of buffer B, and a 2 min wash of 98% buffer B at a flow rate of 450 nl/min. Column temperature was kept at 60°C by a Peltier element containing in-house-developed oven. MS data were acquired with a Top15 data-dependent MS/MS scan method (topN method) for the library and the BoxCar scan method (Meier et al., 2018) for the study samples. Target values for the full scan MS spectra was 3 x 10^6 charges in the 300-1,650 m/z range with a maximum injection time of 55 ms and a resolution of 120,000 at m/z 200. Fragmentation of precursor ions was performed by higher-energy C-trap dissociation (HCD) with a normalized collision energy of 27 eV. MS/MS scans were performed at a resolution of 15,000 at m/z 200 with an ion target value of 5 x 10^4 and a maximum injection time of 25 ms.

Data Analysis

MS raw files were analyzed using the MaxQuant software (Cox and Mann, 2008) and peptide lists were searched against the human Uniprot FASTA database with the Andromeda search engine (Cox et al., 2011). A contaminants database was employed and cysteine carbamidomethylation was set as a fixed modification and N-terminal acetylation and methionine oxidations as variable modifications. False discovery rate (FDR) was 0.01 for both the protein and peptide level with a minimum length of 7 amino acids for peptides and this FDR was determined by searching a reverse sequence database. Enzyme specificity was set as C-terminal to arginine and lysine as expected using trypsin and LysC as proteases, and a maximum of two missed cleavages were allowed. Peptides were identified with an initial precursor mass deviation of up to 7 ppm and a fragment mass deviation of 20 ppm. 'Match between run algorithm' in MaxQuant (Nagaraj et al., 2012) was performed after constructing a matching library consisting of depleted plasma samples. All proteins and peptides matching to the reversed database were filtered out. For label-free protein quantitation (LFQ) we required a minimum ratio count of 2 (Cox et al., 2014). Glycated peptide were identified as previously reported (Keilhauer et al., 2016).

QUANTIFICATION AND STATISTICAL ANALYSIS

All bioinformatic analyses were done with the Perseus software of the MaxQuant computational platform (Cox and Mann, 2008; Tyanova et al., 2016). For statistical analysis of significantly changed proteins before and after RYGB, we used a one-sample t-test with a false discovery rate of <0.05 after Benjamini-Hochberg correction. Correlation to clinical parameters like BMI and insulin resistance data to MS-based proteomic data were also done within the Perseus environment.

Global Correlation Analysis

Proteins were only considered for the analysis, if they were present in at least 25% of all samples, which is equal to 44 out of the 175 measured samples. After removal of potential contaminants like platelet proteins, this left 580 proteins. Peptide glycation: Quantified glycation sites were also filtered for at least 25% valid values and Z-scored over all individuals and time points. The median of this normalized index over 203 glycation sites is reported as the 'peptide glycation' factor.

Inflammation System

We filtered for proteins of the inflammation system by including keywords enriched in the analysis of Figure 2 (complement pathway, immunity, innate immunity, membrane attack complex, cytolysis, complement alternate pathway, inflammatory response, antimicrobial) and further included the term 'acute phase' as it added well-known inflammation proteins like the CRP.

Lipid Homeostasis System

We filtered the plasma proteome for the gene ontology cellular compartment (GOCC) keywords lipid transport, chylomicron, high density lipoprotein (HDL), low density lipoprotein (LDL), intermediate density lipoprotein (IDL) and very low density lipoprotein (vLDL) particles. We further included non-annotated proteins well known to associate with lipid metabolism: apolipoprotein D (APOD), apolipoprotein(a) (LPA), Prolow-density lipoprotein receptor-related protein 1 (LRP1) and phospholipid transfer protein (PLTP), and excluded the keyword annotated inflammation proteins SAA1, SAA2 and SAA4, which are not associated with lipoprotein particles. Filtering for at least 10% valid values, resulted in a set of 25 proteins (Table S9). The median changes of the proteins were calculated across all time points.

Scoring System for Insulin Sensitivity

The correlation analysis were controlled by a Benjamini-Hochberg false discovery rate (FDR) of 0.05 to take multiple hypothesis testing into account. We ranked proteins correlating to the four insulin sensitivity parameters ('homeostatic model assessment of insulin resistance' (HOMA-IR), 'hepatic insulin sensitivity', 'peripheral insulin sensitivity', 'oral glucose insulin sensitivity') according to their Pearson correlation coefficient. The five proteins with the highest correlation to each of the assessments were assigned the score 4, the next five proteins 3, the following five 2 and the rest 1 (Table S8).

Insulin Sensitivity Score

We defined an overall score for each protein adding the individual scores in each of the four insulin sensitivity assays. Next, we normalized the protein trajectories over time, using baseline level before surgery for each individual as 100%. The score weighted the impact of each of the proteins and the median was plotted for both RYGB studies over time.

DATA AND SOFTWARE AVAILABILITY

The MS-based proteomics data have been deposited to the ProteomeXchange Consortium via the PRIDE partner repository and are available via ProteomeXchange with identifier PXD009348.